Available online at www.sciencedirect.com
ScienceDirect
Journal of Sound and Vibration 306 (2007) 580–600
JOURNAL OF SOUND AND VIBRATION
www.elsevier.com/locate/jsvi

Nonlinear vibrations of shallow shells with complex boundary: R-functions method and experiments

Lidia Kurpa[a], Galina Pilgun[a], Marco Amabili[b,*]

[a]*Department of Applied Mathematics, National Technical University "Kharkov Polytechnic Institute", Frunze street 21, Kharkov 61002, Ukraine*
[b]*Dipartimento di Ingegneria Industriale, Università di Parma, Parco Area delle Scienze 181/A, Parma 43100, Italy*

Received 11 January 2007; received in revised form 27 May 2007; accepted 29 May 2007

Abstract

Geometrically nonlinear vibrations of shallow circular cylindrical panels with complex shape of the boundary are considered. The R-functions theory and variational methods are used to study the problem. The R-functions method (RFM) allows constructing in analytical form the sequence of basis functions satisfying the given boundary conditions in case of complex shape of the boundary. The problem is reduced to a single second-order differential equation with quadratic and cubic nonlinear terms. The method developed has been initially applied to study free vibrations of shallow circular cylindrical panels with rectangular base for different boundary conditions: (i) clamped edges, (ii) in-plane immovable simply supported edges, (iii) classically simply supported edges, and (iv) in-plane free simply supported edges. Then, the same approach is applied to a shell with complex shape of the boundary. Experiments have been conducted on an aluminum panel with complex shape of the boundary in order to identify the nonlinear response of the fundamental mode; these experimental results have been compared to numerical results.

1. Introduction

Refs. [1–3] are the most complete reviews of studies on nonlinear vibrations of shallow shells. In pioneering studies [4–9], tangential and rotary inertia were neglected in the dynamics of shallow shells in order to simplify the mathematical formulation. As a rule, the single-mode expansion of the displacements was used to find an approximate solution of the nonlinear partial differential equations of motion. By using variational methods, the initial problem was reduced to a second order, ordinary nonlinear differential equation in the single parameter given by the vibration amplitude. Different methods were applied to integrate the differential equation: the Lindstedt method [6,7], the method of continuation [10], numerical integration [4,7,11,12] and the harmonic balance method [13]. The effect of aspect ratios on nonlinear free vibrations of simply supported

*Corresponding author. Tel.: +39 0521 905896; fax: +39 0521 905705.
E-mail addresses: kurpa@kpi.kharkov.ua (L. Kurpa), PilgunG@kpi.kharkov.ua (G. Pilgun), marco.amabili@unipr.it (M. Amabili).
URL: http://me.unipr.it/mam/amabili/amabili.html (M. Amabili).

0022-460X/$ - see front matter © 2007 Elsevier Ltd. All rights reserved.
doi:10.1016/j.jsv.2007.05.045

circular cylindrical panels with rectangular base was investigated in Ref. [14]; nonlinear vibrations of simply supported circular cylindrical panels subjected to axial excitations were studied in Ref. [15].

In the following years, studies on nonlinear dynamics of shallow shells introduced important refinements: increased number of modes (i.e. degrees of freedom (dof)) in the approximating functions [16–22], use of improved shell theories [1,13,21,23,24] and introduction of physical nonlinearity [25–27].

In order to solve the system of nonlinear partial differential equations, it is necessary to discretize the system, e.g. by using admissible functions. The construction of the basis functions, satisfying the boundary conditions, is a very difficult task in case of complex domains. In fact, a very small number of studies address the nonlinear dynamics of structural elements of complicated geometry. The R-functions theory, developed by the Ukrainian mathematician V.L. Rvachev, is one of the possible approaches to solve the problem [28–33]. It allows building the basis functions in analytical form for an arbitrary domain and different boundary conditions, including mixed boundary conditions.

In the present study, geometrically nonlinear vibrations of shallow circular cylindrical panels with complex shape of the boundary are considered. The present approach is based on the R-functions theory and variational methods. Numerical calculations of nonlinear free vibrations of circular cylindrical panels with rectangular base have been performed for several types of homogeneous boundary conditions: (i) clamped edges, (ii) in-plane immovable simply supported edges, (iii) classically simply supported edges and (iv) in-plane free simply supported edges. A comparison is carried out with the results previously reported by Amabili [21,34] for the response of circular cylindrical panels to harmonic excitation in the frequency neighborhood of the fundamental mode. Nonlinear free vibrations of simply supported circular cylindrical panels with complex shape of the boundary have been investigated by using the R-functions method (RFM). Experiments have been conducted on an aluminum shell with complex shape of the boundary in order to identify the nonlinear response of the fundamental mode; these experimental results have been compared to numerical results.

2. Problem formulation

A shallow shell of uniform thickness h and arbitrary shape is considered; it is assumed that the deflection of its middle surface is of the same order of the shell thickness. The principal lines of curvature of the middle surface coincide with the coordinates x, y of the Cartesian coordinate system, and z is direct along the normal to the middle surface of the shell and is oriented inwards, as shown in Fig. 1. Strain–displacement relationships based on the Donnell–Mushtary–Vlasov nonlinear shell theory [4] are used in the present study. The middle surface strains ε_x, ε_y, ε_{xy} and the changes in curvature and torsion χ_x, χ_y, χ_{xy} of a doubly-curved shallow shell are given by

$$\varepsilon_x = \frac{\partial u}{\partial x} - \frac{w}{R_x} + \frac{1}{2}\left(\frac{\partial w}{\partial x}\right)^2, \quad \varepsilon_y = \frac{\partial v}{\partial y} - \frac{w}{R_y} + \frac{1}{2}\left(\frac{\partial w}{\partial y}\right)^2, \quad \gamma_{xy} = \frac{\partial u}{\partial y} + \frac{\partial v}{\partial x} + \frac{\partial w}{\partial x}\frac{\partial w}{\partial y}, \tag{1}$$

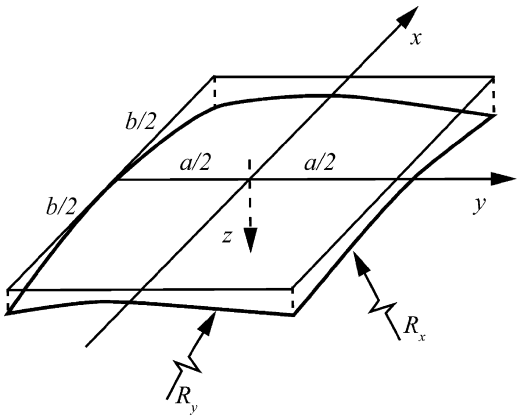

Fig. 1. Geometry of the shallow shell and coordinate system.

$$\chi_x = -\frac{\partial^2 w}{\partial x^2}, \quad \chi_y = -\frac{\partial^2 w}{\partial y^2}, \quad \chi_{xy} = -2\frac{\partial^2 w}{\partial x \partial y}, \tag{2}$$

where u, v, w are the displacements of an arbitrary point on the middle surface in x, y, z directions, respectively, and R_x, R_y are the constant middle surface principal radii of curvature in x, y directions, respectively.

The following equations of motion, according to the Donnell–Mushtary–Vlasov nonlinear shell theory, are used [4]:

$$\frac{\partial^2 \bar{u}}{\partial \xi^2} + \frac{1-\mu}{2}\frac{\partial^2 \bar{u}}{\partial \eta^2} + \frac{1+\mu}{2}\frac{\partial^2 \bar{v}}{\partial \xi \partial \eta} = l_1(\bar{w}) + Nl_1(\bar{w}) + \lambda^2 \frac{h^2}{a^2}\frac{\partial^2 \bar{u}}{\partial \tau^2}, \tag{3}$$

$$\frac{1+\mu}{2}\frac{\partial^2 \bar{u}}{\partial \xi \partial \eta} + \frac{1-\mu}{2}\frac{\partial^2 \bar{v}}{\partial \xi^2} + \frac{\partial^2 \bar{v}}{\partial \eta^2} = l_2(\bar{w}) + Nl_2(\bar{w}) + \lambda^2 \frac{h^2}{a^2}\frac{\partial^2 \bar{v}}{\partial \tau^2}, \tag{4}$$

$$\begin{aligned}\frac{1}{12}\nabla^4 \bar{w} - \left(K_\xi + \mu K_\eta\right)\frac{\partial \bar{u}}{\partial \xi} - \left(\mu K_\xi + K_\eta\right)\frac{\partial \bar{v}}{\partial \eta} + \left(K_\xi^2 + K_\eta^2 + 2\mu K_\xi K_\eta\right)\bar{w} \\ = \frac{K_\xi + \mu K_\eta}{2}\left(\frac{\partial \bar{w}}{\partial \xi}\right)^2 + \frac{K_\eta + \mu K_\xi}{2}\left(\frac{\partial \bar{w}}{\partial \eta}\right)^2 + \frac{\partial^2 \bar{w}}{\partial \xi^2}N_\xi + (1-\mu)\frac{\partial^2 \bar{w}}{\partial \xi \partial \eta}T + \frac{\partial^2 \bar{w}}{\partial \eta^2}N_\eta - \lambda^2 \frac{\partial^2 \bar{w}}{\partial \tau^2},\end{aligned} \tag{5}$$

where $\nabla^4 = (\partial^4/\partial \xi^4) + 2(\partial^4/\partial \xi^2 \partial \eta^2) + (\partial^4/\partial \eta^4)$ is the biharmonic operator, and the linear and nonlinear operators $l_1(\bar{w})$, $l_2(\bar{w})$, $Nl_1(\bar{w})$, and $Nl_2(\bar{w})$ are given by

$$l_1(\bar{w}) = \left(K_\xi + \mu K_\eta\right)\frac{\partial \bar{w}}{\partial \xi}, \quad l_2(\bar{w}) = \left(\mu K_\xi + K_\eta\right)\frac{\partial \bar{w}}{\partial \eta}, \tag{6a,b}$$

$$Nl_1(\bar{w}) = -\frac{\partial \bar{w}}{\partial \xi}\left(\frac{\partial^2 \bar{w}}{\partial \xi^2} + \frac{1-\mu}{2}\frac{\partial^2 \bar{w}}{\partial \eta^2}\right) - \frac{1+\mu}{2}\frac{\partial \bar{w}}{\partial \eta}\frac{\partial^2 \bar{w}}{\partial \xi \partial \eta}, \tag{7}$$

$$Nl_2(w) = -\frac{\partial \bar{w}}{\partial \eta}\left(\frac{\partial^2 \bar{w}}{\partial \eta^2} + \frac{1-\mu}{2}\frac{\partial^2 \bar{w}}{\partial \xi^2}\right) - \frac{1+\mu}{2}\frac{\partial \bar{w}}{\partial \xi}\frac{\partial^2 \bar{w}}{\partial \xi \partial \eta}. \tag{8}$$

Equations of motion (3–5) include in-plane inertia but neglect rotary inertia and shear deformation; this is a good approximation for uniform thin shells. In expressions (3–5) the following non-dimensional variables have been introduced:

$$\xi = \frac{x}{a}, \ \eta = \frac{y}{a}, \ \bar{u} = \frac{ua}{h^2}, \ \bar{v} = \frac{va}{h^2}, \ \bar{w} = \frac{w}{h}, \ \bar{\tau} = \omega_0 t, \ K_\eta = \frac{a^2}{R_y h}, \ K_\xi = \frac{a^2}{R_x h}, \tag{9}$$

where a is the characteristic size of the base of the panel, E is Young's modulus, μ is the Poisson ratio, ρ is the mass density, t is time and ω_0 is the natural circular frequency of the mode considered, which is related to the non-dimensional frequency parameter λ as follows:

$$\omega_0 = \frac{\lambda}{a^2}\sqrt{\frac{Eh^2}{\rho(1-\mu^2)}}. \tag{10}$$

The non-dimensional forces per unit length N_ξ, N_η, T are given by a linear and a nonlinear part (hereafter the overline on the non-dimensional displacements is omitted for simplicity):

$$N_\xi(u,v,w) = N_\xi^L(u,v,w) + N_\xi^D(w), \quad N_\eta(u,v,w) = N_\eta^L(u,v,w) + N_\eta^D(w), \tag{11a,b}$$

$$T(u,v,w) = T^L(u,v) + T^D(w), \tag{11c}$$

where

$$N_{\xi}^{L}(u,v,w)=\frac{\partial u}{\partial \xi}+\mu\frac{\partial v}{\partial \eta}-\left(K_{\xi}+\mu K_{\eta}\right)w,\quad N_{\eta}^{L}(u,v,w)=\mu\frac{\partial u}{\partial \xi}+\frac{\partial v}{\partial \eta}-\left(\mu K_{\xi}+K_{\eta}\right)w, \tag{12a,b}$$

$$T^{L}(u,v)=\frac{\partial u}{\partial \eta}+\frac{\partial v}{\partial \xi}, \tag{12c}$$

$$N_{\xi}^{D}(w)=\frac{1}{2}\left(\frac{\partial w}{\partial \xi}\right)^{2}+\frac{\mu}{2}\left(\frac{\partial w}{\partial \eta}\right)^{2},\quad N_{\eta}^{D}(w)=\frac{1}{2}\left(\frac{\partial w}{\partial \eta}\right)^{2}+\frac{\mu}{2}\left(\frac{\partial w}{\partial \xi}\right)^{2},\quad T^{D}(w)=\frac{\partial w}{\partial \xi}\frac{\partial w}{\partial \eta}. \tag{13a–c}$$

In the limit case of a flat plate, for which $K_{\xi}=K_{\eta}=0$, N_{ξ}, N_{η} are denoted as N_{ξ}^{PL}, N_{η}^{PL}, and take the simplified expressions:

$$N_{\xi}^{PL}(u,v,w)=\frac{\partial u}{\partial \xi}+\mu\frac{\partial v}{\partial \eta}+\frac{1}{2}\left(\frac{\partial w}{\partial \xi}\right)^{2}+\frac{\mu}{2}\left(\frac{\partial w}{\partial \eta}\right)^{2},$$

$$N_{\eta}^{PL}(u,v,w)=\frac{\partial v}{\partial \eta}+\mu\frac{\partial u}{\partial \xi}+\frac{1}{2}\left(\frac{\partial w}{\partial \eta}\right)^{2}+\frac{\mu}{2}\left(\frac{\partial w}{\partial \xi}\right)^{2}. \tag{14a, b}$$

Four boundary conditions are given at each edge of the panel. The boundary conditions considered in this study are:

– Clamped panel:

$$u_n=0,\quad v_n=0,\quad w=\frac{\partial w}{\partial n}=0, \tag{15}$$

where $u_n=ul+vm$, $v_n=-um+vl$, and l, m are the direction cosines of the edge with respect to the in-plane coordinates u, v (in case of curved edge, l and m are functions of the position); n, τ are the normal and the tangent to the boundary, respectively; both of them are contained in the plane tangent to the panel at the boundary, with the normal directed outward the shell domain.

– In-plane immovable simply supported panel:

$$u_n=0\quad v_n=0,\quad w=0,\quad M_n=-D\left(\frac{\partial^2 w}{\partial n^2}+\mu\frac{\partial^2 w}{\partial \tau^2}\right)=0, \tag{16}$$

where M_n is the bending moment.

– Classical simply supported panel:

$$v_n=0,\quad w=0,\quad N_n=0,\quad M_n=0. \tag{17}$$

– In-plane free simply supported panel:

$$N_n=0,\quad N_{n\tau}=0,\quad w=0,\quad M_n=0, \tag{18}$$

where $N_n=N_{\xi}l^2+N_{\eta}m^2+2Tlm$, $N_{n\tau}=T(l^2-m^2)+(N_{\eta}-N_{\xi})\,lm$.

– In-plane free simply supported panel with elastic distributed springs tangent to the edges:

$$N_n=0,\quad N_{n\tau}=-k_{\mathrm{spr}}v_n,\quad w=0,\quad M_n=0. \tag{19}$$

where k_{spr} is the spring stiffness per unit length.

3. Solution method

Let us assume that the vectorial eigenfunction $\vec{U}=(U_1,V_1,W_1)$ associated with the fundamental natural frequency of free vibrations is known; the procedure to determinate $\vec{U}$ is presented in Section 5 and is carried

out by using the RFM. The deflection $w(\xi,\eta,\bar{\tau})$ is assumed to be expressed by

$$w(\xi,\eta,\bar{\tau}) = y_1(\bar{\tau})W_1(\xi,\eta), \tag{20}$$

where $W_1(\xi,\eta)$ is a component of the vectorial eigenfunction; this is a single-mode expansion. Eq. (20) is an approximation, which is a limitation of the present study; numerical results show that this approximation can give accurate results for thin shallow panels with weak nonlinearity, in absence of internal resonances.

The in-plane displacements u and v are expanded by taking into account that the functions $u(\xi,\eta,\bar{\tau})$ and $v(\xi,\eta,\bar{\tau})$ must satisfy identically Eqs. (3) and (4), and the boundary conditions. By substituting Eq. (20) into Eqs. (3) and (4) where in-plane inertia is neglected (i.e. the last term on the right-hand side is deleted in Eqs. (3) and (4)), one obtains a system of equations having the following solution:

$$u(\xi,\eta,\bar{\tau}) = y_1(\bar{\tau})U_1(\xi,\eta) + y_1^2(\bar{\tau})U_2(\xi,\eta), \tag{21}$$

$$v(\xi,\eta,\bar{\tau}) = y_1(\bar{\tau})V_1(\xi,\eta) + y_1^2(\bar{\tau})V_2(\xi,\eta), \tag{22}$$

In Eqs. (21) and (22), U_1 and V_1 are the first two components of the vectorial eigenfunction $\vec{U}$ previously defined, and U_2 and V_2 are the solution of the system of equations (3) and (4) with, on the right-hand side, only the nonlinear terms given by Eqs. (7), and (8) (i.e. canceling the linear terms and in-plane inertia); U_2 and V_2 satisfy the appropriate boundary conditions. The method developed to obtain U_2 and V_2 is described in Section 6.

By substituting U_1, V_1, U_2, V_2, W_1 into Eq. (5) and applying the Galerkin method, a second-order nonlinear differential equation in the time function $y_1(\tau)$ is obtained in the form:

$$y_1''(\bar{\tau}) + y_1(\bar{\tau}) - \alpha y_1^2(\bar{\tau}) + \beta y_1^3(\bar{\tau}) = 0. \tag{23}$$

The quadratic and cubic coefficients α and β are given by

$$\alpha = -\frac{\int_\Omega \Big\{ K_\xi N_\xi^{PL}(U_2,V_2,W_1) + K_\eta N_\eta^{PL}(U_2,V_2,W_1) - N_\xi^L(U_1,V_1,W_1)W_{1,\xi\xi} - N_\eta^L(U_1,V_1,W_1)W_{1,\eta\eta} - (1-\mu)T^L(U_1,V_1)W_{1,\xi\eta} \Big\} W_1 \,\mathrm{d}\Omega}{\lambda^2 \|W_1\|^2}, \tag{24}$$

$$\beta = -\frac{\int_\Omega \Big\{ W_{1,\xi\xi} N_\xi^{PL}(U_2,V_2,W_1) + (1-\mu)W_{1,\xi\eta}T(U_2,V_2,W_1) + W_{1,\eta\eta}N_\eta^{PL}(U_2,V_2,W_1) \Big\} W_1 \,\mathrm{d}\Omega}{\lambda^2 \|W_1\|^2}, \tag{25}$$

where the subscript "," indicates a partial derivative, $N_\xi{}^L$, $N_\eta{}^L$, T^L are defined by Eqs. (12a–c), and N, $N_\xi{}^{PL}$, $N_\eta{}^{PL}$ are defined by Eqs. (14a,b). In case of a flat plate, Eq. (23) becomes simpler, due to $K_\xi = K_\eta = 0$, and $\alpha = 0$. Equation (23) can be integrated by using numerical methods.

4. The RFM

The RFM [28,29,35,36] allows searching for a solution of boundary value problems in a form that satisfies exactly all the boundary conditions and contains functions to be determined in order to satisfy the differential equations governing the problem in approximate way. Kantorovitch [37] introduced a solution u to homogeneous Dirichlet conditions:

$$u|_{\partial\Omega} = 0, \tag{26}$$

where $\partial\Omega$ is the boundary of the domain; this solution has the form:

$$u = \omega P, \tag{27a}$$

where the function ω vanishes at the boundary ($\omega|_{\partial\Omega} = 0$) and is positive in the interior of Ω, and P is an unknown function which allows to satisfy the differential equations governing the problem. Since ω is identically zero at the boundary $\partial\Omega$, then no matter what the indefinite component P (differentiable up to the required order) is, the function u given by Eq. (27a) will satisfy the boundary condition (26) exactly.

The function P is determined in order to satisfy the differential equations; therefore, in general, it can be expressed in approximate way by using a series expansion of basis functions ψ_i:

$$P = \sum_{i=1}^{N} C_i \psi_i, \tag{27b}$$

where C_i are scalar coefficients. Thus, the solution takes the form:

$$u = \omega \sum_{i=1}^{N} C_i \psi_i. \tag{28}$$

The undetermined coefficients C_i can be found numerically, e.g. by using variational or Galerkin methods.

This idea of Kantorovitch did not have particular success because: (i) there was no available technique to construct such real functions ω for complex domains and (ii) the same solution was not applicable to other types of boundary value problems.

Rvachev [28,38] found the way to overcome both of the obstacles by creating the R-functions theory. R-functions are elementary functions f whose sign is completely defined by the sign of their arguments; i.e. for any R-function f exists a Boolean function $F(X_1, X_2, \ldots, X_n)$ of Boolean variables X_n which satisfies the following equality $F(S_2(x_1), S_2(x_2), \ldots S_2(x_n)) = S_2(f(x_1, x_2, \ldots, x_n))$. The two-valued predicate $S_2(x)$ is defined by

$$S_2(x) = \begin{cases} 0, & \forall\, x < 0, \\ 1, & \forall\, x \geqslant 0. \end{cases} \tag{29}$$

Functions that satisfy this properties are e.g. xyz, $x + y + \sqrt{xy + x^2 + y^2}$ and $xy + z + |z - xy|$. R-functions behave as continuous analogs of logical Boolean functions. Every Boolean function has infinity analog R-functions. The most known system of R-functions is given by the R-conjunction $(x \wedge_\alpha y)$ and the R-disjunction $(x \vee_\alpha y)$, which are defined as

$$x \wedge_\alpha y = \frac{1}{1+\alpha}\left(x + y - \sqrt{x^2 + y^2 - 2\alpha xy}\right), \tag{30}$$

$$x \vee_\alpha y = \frac{1}{1+\alpha}\left(x + y + \sqrt{x^2 + y^2 - 2\alpha xy}\right), \tag{31}$$

where α is a continuous function satisfying the condition $-1 < \alpha(x, y) \leqslant 1$; the denial function, simply given by minus "$-$", must be added to complete this system of R-functions. The R-conjunction (30) is an R-function whose companion Boolean function is logical "and"$(\wedge)$, whereas Eq. (31) has companion Boolean function logical "or" $(\vee)$. Note that the precise value of α is not important in many applications, and often it is set to a constant. If $\alpha = 1$ is taken, Eqs. (30) and (31) become the functions $\mathrm{Min}(x, y)$ and $\mathrm{Max}(x, y)$, respectively. Setting $\alpha = 0$ in Eqs. (30) and (31), the following simpler functions are obtained:

$$x \wedge_0 y = x + y - \sqrt{x^2 + y^2}, \tag{32}$$

$$x \vee_0 y = x + y + \sqrt{x^2 + y^2}. \tag{33}$$

R-functions are closed under composition; therefore the function ω can be obtained for complex domains (eventually time-varying), which can be represented by using primitive geometric regions, e.g. defined by systems of inequalities. Using R-operations, such as R-disjunctions $(x \vee_\alpha y)$, which has analog Boolean union $\cup$, and R-conjunction $(x \wedge_\alpha y)$, with analog Boolean intersection $\cap$, it is possible to construct the analytical expression of ω for any domain Ω.

The first step in order to build ω for the domain $\Omega = \Omega(Q)$, where Q is a point in the plane (x, y) or in a three-dimensional space, it is necessary to construct the so-called characteristic function (also named

two-valued predicate) of the domain Ω, which is defined as

$$\Omega = \Omega(Q) = \begin{cases} 0, & \forall\ Q \notin \Omega, \\ 1, & \forall\ Q \in \Omega. \end{cases} \tag{34}$$

Usually the domain and its characteristic function are denoted with the same symbol.

In general, the characteristic function of the domain Ω is obtained by applying simple operations $\vee$, $\wedge$, $-$, that correspond to the Boolean operations union $\cup$, intersection $\cap$ and absolute complement $^{-}$, to sub-domains Ω_i. A characteristic function Ω_i can be defined for each sub-domain Ω_i:

$$\Omega_i(Q) = \begin{cases} 0, & \forall\ Q \notin \Omega_i, \\ 1, & \forall\ Q \in \Omega_i. \end{cases} \tag{35}$$

Since $\Omega_i \in B_2\{0, 1\}$, i.e. to the space of Boolean functions, then Ω_i may be used as an arguments of the Boolean function F:

$$\Omega = F(\Omega_1, \Omega_2, \ldots, \Omega_n), \tag{36}$$

which is the characteristic function of the domain Ω. It is obvious that the domain Ω is determined not only by the shape of sub-domains Ω_i, but also by the type of Boolean functions involved in F (union, intersection and absolute complement).

As next step in the determination of ω, the function η_i is introduced as the continuous analog of the characteristic function Ω_i and is defined as

$$\begin{aligned} &\eta_i(Q) > 0 \quad \forall\ Q \in \Omega_i, \\ &\eta_i(Q) < 0 \quad \forall\ Q \notin \Omega_i, \\ &\eta_i(Q) = 0 \quad \forall\ Q \in \partial\Omega_i. \end{aligned} \tag{37}$$

Let us assume that the domain Ω is defined by the characteristic function (two-valued predicate) represented in Eq. (36), where $F(\Omega_1, \ldots, \Omega_n)$ is a known Boolean function. Then the inequality $f(\eta_1, \ldots, \eta_n) \geqslant 0$ describes the domain Ω, where $\omega = f(\eta_1, \ldots, \eta_n)$ is an R-function that corresponds to the Boolean function $F(\Omega_1, \ldots, \Omega_n)$. To construct the function $\omega(x, y)$ it is sufficient to perform a formal substitution of the characteristic function Ω_i with the continuous function η_i and the Boolean operations $\Omega_i \cap \Omega_j$, $\Omega_i \cup \Omega_j$, $\bar{\Omega}_i$, (intersection, union and absolute complement) with the corresponding symbols of R-operations, $\eta_i \wedge_\alpha \eta_j$, $\eta_i \vee_\alpha \eta_j$, $-\eta_i$. Following this substitution, the continuous function ω of the domain Ω is given by

$$\omega = f(\eta_1, \eta_2, \ldots, \eta_n). \tag{38}$$

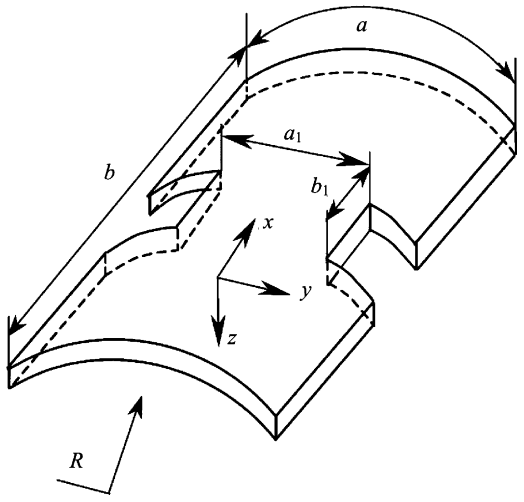

Fig. 2. Panel with complex shape of the boundary and coordinate system.

In order to better understand the method, the function ω is built for the panel studied in Section 7.2 and shown in Fig. 2. The domain Ω representing the panel surface is given by following Boolean operations on sub-domains Ω_i:

$$\Omega = \Omega_1 \wedge \Omega_2 \wedge (\Omega_3 \vee \Omega_4), \tag{39}$$

by using (39), the equation of the domain for the panel in Fig. 2 may be written as

$$\omega(x,y) = \eta_1 \wedge_0 \eta_2 \wedge_0 (\eta_3 \vee_0 \eta_4), \tag{40a}$$

where the functions η_i, $i = 1,\ldots,4$, are given by

$$\eta_1 = \left(\left(\frac{b}{2}\right)^2 - x^2\right)/b \geqslant 0 \text{ in } \Omega_1, \quad \eta_2 = \left(\left(\frac{a}{2}\right)^2 - y^2\right)/a \geqslant 0 \text{ in } \Omega_2, \tag{40b}$$

which are associated to horizontal (Ω_1) and vertical (Ω_2) strips in the plane comprised between the straight lines $x = \pm b/2$ and $y = \pm a/2$, respectively,

$$\eta_3 = \left(\left(\frac{a_1}{2}\right)^2 - y^2\right)/a_1 \geqslant 0 \text{ in } \Omega_3, \quad \eta_4 = \left(x^2 - \left(\frac{b_1}{2}\right)^2\right)/b_1 \geqslant 0 \text{ in } \Omega_4, \tag{40c}$$

in particular, Ω_3 is a vertical strip between $y = \pm a_1/2$ and Ω_4 is the region of the plane exterior to the horizontal strip delimited by $x = \pm b_1/2$.

Eq. (40a) is normalized up to the first order, i.e. satisfies the following conditions:

$$\omega(x,y) = 0, \quad \forall (x,y) \in \partial\Omega, \tag{41a}$$

$$\frac{\partial \omega}{\partial n} = -1, \quad \forall (x,y) \in \partial\Omega. \tag{41b}$$

Inside the domain Ω, the inequality $\omega(x,y) > 0$ is verified.

It is possible to extend the solution procedure of Eq. (27) to the case of inhomogeneous Dirichlet conditions given by

$$u|_{\partial\Omega} = \varphi_0, \tag{42}$$

where φ_0 is a function defined at the boundary $\partial\Omega$ and φ is its extension defined in all the domain Ω. The solution structure can be written in the following form:

$$u = \omega P + \varphi. \tag{43}$$

The general case of inhomogeneous Dirichlet conditions, in which the function φ_0 in Eq. (42) is specified as a piecewise function at the boundary $\partial\Omega$, can be solved by using the generalized Lagrange formula obtained by Rvachev. The function φ_0 on the section $\partial\Omega_i$ of the boundary $\partial\Omega$ of the domain Ω is indicated as

$$\varphi_0(x,y)\big|_{\partial\Omega_i} = \varphi_i. \tag{44}$$

Then solution may be represented by using the generalized Lagrange formula [28]:

$$u = \omega^k P + \frac{\sum_{i=1}^{n} \varphi_i \omega_i^{-k_i}}{\sum_{i=1}^{n} \omega_i^{-k_i}}, \quad \text{with } k_i \geqslant 1 \text{ and } k = \max(k_i). \tag{45}$$

Solution (45) is given by a set of functions taking the given values φ_i on the respective sections of the boundary $\partial\Omega$; a possible choice is $k = k_i = 1$, which makes the solution defined everywhere except at corner points. If $k_i > 1$, the partial derivatives of the function u coincide on the section $\partial\Omega_i$ with the corresponding partial derivatives of the functions φ_i up to the $k_i - 1$ order. Eq. (45) may be considered as the general solution structure for inhomogeneous Dirichlet problems.

Differential operators have been introduced by Rvachev to take into account boundary conditions of differential type. For example, for two-dimensional problems, these operators have the following form:

$$D_k = \sum_{i=0}^{k} C_k^i \left(\frac{\partial\omega}{\partial x}\right)^{k-i} \left(\frac{\partial\omega}{\partial y}\right)^{i} \frac{\partial^k}{\partial x^{k-i}\partial y^i}, \tag{46a}$$

$$T_k = \sum_{i=0}^{k} (-1)^{k-i} C_k^i \left(\frac{\partial\omega}{\partial x}\right)^{i} \left(\frac{\partial\omega}{\partial y}\right)^{k-i} \frac{\partial^k}{\partial x^{k-i}\partial y^i}, \tag{46b}$$

where $C_k^i = k(k-1)\ldots(k-i+1)/i!$, and $k \geqslant 1$; $\omega(x, y) = 0$ is, as usual, the normalized equation of $\partial\Omega$ (or of a section $\partial\Omega_i$). Any function $u(x, y) \in C^n(\Omega)$ satisfy the following expressions:

$$D_k(u) = \frac{\partial^k u}{\partial n^k}, \quad T_k(u) = \frac{\partial^k u}{\partial \tau^k}, \quad \forall\ (x, y) \in \partial\Omega, \tag{46c,d}$$

$$(T_{k-m}D_m)(u) = (D_m T_{k-m})(u) = \frac{\partial^k u}{\partial n^m \partial \tau^{k-m}}, \quad \forall\ (x, y) \in \partial\Omega, \tag{46e}$$

where n and τ are here the outward normal and tangent to the boundary, respectively.

In case of Neumann boundary conditions in the form:

$$\left.\frac{\partial u}{\partial n}\right|_{\partial\Omega} = \varphi_0, \tag{47}$$

the solution structure can be written in the following form:

$$u = P + \omega\varphi - \omega D_1(P) + \omega^2 P, \tag{48a}$$

where P and φ have been previously built for Dirichlet conditions and D_1 is given by Eq. (46a) for $k = 1$; Eq. (48a) is based on the generalized Taylor series [36]. Similar procedures can be used for virtually any boundary condition, included mixed boundary conditions. In particular, for boundary condition of the type $u|_{\partial\Omega} = \partial u/\partial n\big|_{\partial\Omega} = 0$, which are those of clamped edges, the solution structure can be written in the following form:

$$u = \omega^2 P. \tag{48b}$$

The structure of admissible functions corresponding to clamped edges, Eq. (15), and in-plane immovable simply supported edges, Eq. (16), is

$$U_1 = \omega P_1, \quad V_1 = \omega P_2, \quad W_1 = \omega^k P_3, \tag{49}$$

where $\omega = 0$ is the normalized equation of the domain boundary; the parameter k in Eq. (49) depends on the type of boundary condition: $k = 1$ for simply supported edges and $k = 2$ for clamped edges. The following structure of the solution satisfies the classical simply supported edges, Eq. (17),

$$U_1 = \frac{\partial\omega}{\partial x} P_2 + \omega P_3, \quad V_1 = \frac{\partial\omega}{\partial y} P_2 + \omega P_4, \quad W_1 = \omega P_1. \tag{50}$$

If the edges of the panel base are parallel to the coordinates axes, Eq. (50) can be rewritten into a simpler form. As $\partial\omega/\partial x = 0$ on the sides parallel to the axis x, and $\partial\omega/\partial y = 0$ on the sides parallel to y, Eq. (50) take the simplified form:

$$U_1 = \omega_1 P_3, \quad V_1 = \omega_2 P_4, \quad W_1 = \omega P_1, \tag{51}$$

where $\omega_i = 0\ (i = 1, 2)$ are the equations of the domain edges on which the boundary conditions $U_1 = 0$ or $V_1 = 0$, respectively, should be satisfied.

If the panel has in-plane free simply supported edges, Eq. (18), the structure of the solution satisfying the kinematic boundary conditions is

$$U_1 = P_1, \quad V_1 = P_2, \quad W_1 = \omega P_3. \tag{52}$$

In the case of boundary conditions represented by Eq. (19), the structure of the solution satisfying all the boundary conditions is

$$U_1 = P_1\left(1 - m^2 C_{\text{spr}}\omega\right) - \omega\left[D_1 P_1 - lm(1+\mu)T_1 P_1 + \left(\mu l^2 - m^2\right)T_1 P_2 - lmC_{\text{spr}}P_2\right], \tag{53a}$$

$$V_1 = P_2\left(1 - l^2 C_{\text{spr}}\omega\right) - \omega\left[D_1 P_2 + lm(1+\mu)T_1 P_2 + \left(l^2 - \mu m^2\right)T_1 P_1 - lmC_{\text{spr}}P_1\right], \tag{53b}$$

$$W_1 = P_3\left(\omega + \frac{1}{3}\tilde{\omega}\right) + \omega\left(h_1\frac{\partial P_3}{\partial x} + h_2\frac{\partial P_3}{\partial y}\right), \tag{53c}$$

where D_1 and T_1 are obtained by Eq. (46), $C_{\text{spr}} = 2(1+\mu)k_{\text{spr}}/E$, $\omega = \omega(x,y)$ as usual, $\tilde{\omega} = \omega(x+h_1, y+h_2)$ and:

$$h_1 = -\omega\left[x + \frac{1}{2}\omega(x,y),\ \ y\right] + \omega\left[x - \frac{1}{2}\omega(x,y),\ \ y\right],$$
$$h_2 = -\omega\left[x,\ \ y + \frac{1}{2}\omega(x,y)\right] + \omega\left[x,\ \ y - \frac{1}{2}\omega(x,y)\right].$$

In Eqs. (49–53) the functions P_i, $i = 1, \ldots, 4$, are the unknown functions that are represented as

$$P_1(x,y) = \sum_{i=1}^{M_1} a_i\varphi_i(x,y), \quad P_2(x,y) = \sum_{i=M_1+1}^{M_2} a_i\chi_i(x,y),$$
$$P_3(x,y) = \sum_{i=M_2+1}^{M_3} a_i\psi_i(x,y), \quad P_4(x,y) = \sum_{i=M_3+1}^{M_4} a_i\theta_i(x,y). \tag{54a–d}$$

In Eqs. (54) a_i, $i = 1, \ldots, M_4$, are the coefficients defined in Eq. (27b) as C_i, to be determined by solving the corresponding variational problem, and $\varphi_i(x,y)$, $\chi_i(x,y)$, $\psi_i(x,y)$, $\theta_i(x,y)$ are elements of a complete function system $\{\varphi_i(x,y)\}$, $\{\chi_i(x,y)\}$, $\{\psi_i(x,y)\}$, $\{\theta_i(x,y)\}$. For example, the power polynomials, the Chebyshev polynomials, the Legendre polynomials, trigonometric polynomials and functions, or finite functions (splines, atomic functions) can be used in Eqs. (54).

5. Eigenvalue problem for linear vibrations of shallow shells with an arbitrary shape of the boundary by using the R-functions method

Only linear terms are considered here in the shell middle surface strain–displacement relationships (1):

$$\varepsilon_x = \frac{\partial u}{\partial x} - \frac{w}{R_x}, \quad \varepsilon_y = \frac{\partial v}{\partial y} - \frac{w}{R_y}, \quad \gamma_{xy} = \frac{\partial u}{\partial y} + \frac{\partial v}{\partial x}. \tag{55}$$

The solution of Eqs. (3)–(5), after elimination of nonlinear terms, with any of the boundary conditions given by Eqs. (15)–(19) may be reduced to a variational problem by considering the minimum of the Lagrangian, which represents the difference of kinetic and elastic strain energies of the shell, once the displacements are expanded by using admissible functions.

Vibrations are assumed to be harmonic in time, which yields:

$$u_1(\xi,\eta,\bar{\tau}) = U_1(\xi,\eta)\cos\bar{\tau}, \ \ v_1(\xi,\eta,\bar{\tau}) = V_1(\xi,\eta)\cos\bar{\tau}, \ \ W_1(\xi,\eta,\bar{\tau}) = W_1(\xi,\eta)\cos\bar{\tau}. \tag{56}$$

The non-dimensional functional of energy can be written as

$$I=\frac{1}{2}\int_{\Omega}\left\{\left[\left(\frac{\partial U_1}{\partial\xi}-K_\xi W_1\right)^2+2\mu\left(\frac{\partial U_1}{\partial\xi}-K_\xi W_1\right)\left(\frac{\partial V_1}{\partial\eta}-K_\eta W_1\right)+\left(\frac{\partial V_1}{\partial\eta}-K_\eta W_1\right)^2+\frac{1-\mu}{2}\left(\frac{\partial V_1}{\partial\xi}+\frac{\partial U_1}{\partial\eta}\right)\right]+\frac{1}{12}\left[\left(\frac{\partial^2 W_1}{\partial\xi^2}\right)^2+2\mu\frac{\partial^2 W_1}{\partial\xi^2}\frac{\partial^2 W_1}{\partial\eta^2}+\left(\frac{\partial^2 W_1}{\partial\eta^2}\right)^2+(1-\mu)\left(\frac{\partial^2 W_1}{\partial\xi\partial\eta}\right)^2\right]-\frac{\lambda^2}{2}\left(\frac{h^2}{a^2}U_1^2+\frac{h^2}{a^2}V_1^2+W_1^2\right)\right\}\mathrm{d}\Omega, \tag{57}$$

where Ω is the panel surface projection on $\xi\eta$ plane.

The systems of admissible functions must be constructed in order to minimize the functional (57). The R-functions theory is applied in order to find admissible functions for the displacements U_1, V_1, W_1 which satisfy the given boundary conditions [28–31].

In the present study, power polynomials have been used in Eqs. (54) to obtain numerical results. For the panel in Fig. 2, assuming simply supported edges (50, 51), due to the symmetry of the problem in x and y, the following polynomials have been used:

$$\{\varphi_i\}:\ \ 1,x^2,y^2,x^4,x^2y^2,y^4,\ldots, \tag{58a}$$

$$\{\chi_i\}:\ \ x,y,xy,x^3y,xy^3,\ldots, \tag{58b}$$

$$\{\psi_i\}:\ \ y,x^2y,y^3,x^4y,x^2y^3,y^5,\ldots, \tag{58c}$$

$$\{\theta_i\},\ \ x,x^3,xy^2,x^5,x^3y^2,xy^4,\ldots. \tag{58d}$$

By substituting Eqs. (54) into any of the Eqs. (49)–(53) yields:

$$U_1\cong\sum_{i=1}^{N_1}a_iU_{1i},\quad V_1\cong\sum_{i=1+N_1}^{N_2}a_iV_{1i},\quad W_1\cong\sum_{i=1+N_2}^{N_3}a_iW_{1i}, \tag{59a–c}$$

where U_{1i}, V_{1i}, W_{1i} are admissible functions that satisfies the geometrical (kinematical) boundary conditions.

The calculation of the unknown coefficients a_i is carried out by minimizing the Lagrange functional (57):

$$\frac{\partial I}{\partial a_i}=0,\quad i=1,\ldots,N_3, \tag{60}$$

which yields the eigenvalue problem:

$$(\mathbf{K}-\lambda^2\mathbf{M})\mathbf{X}=0, \tag{61}$$

where λ are the eigenvalues, $\mathbf{X}=(a_1,a_2,\ldots,a_{N_3})^{\mathrm{T}}$ are the corresponding eigenvectors, i.e. the vectors of the unknown coefficients, $\mathbf{K}=\{k_{ij}\}_{i,j=1,\ldots,N_3}$ is the stiffness matrix and $\mathbf{M}=\{m_{ij}\}_{i,j=1,\ldots,N_3}$ is the mass matrix.

6. Calculation of U_2 and V_2 in the in-plane expansions

As discussed in Section 2, the functions $U_2(\xi,\eta)$ and $V_2(\xi,\eta)$ are obtained by solving the following differential equations obtained from Eqs. (3) and (4) canceling the linear terms and inertia on the right-hand side:

$$\frac{\partial^2U_2}{\partial\xi^2}+\frac{1-\mu}{2}\frac{\partial^2U_2}{\partial\eta^2}+\frac{1+\mu}{2}\frac{\partial^2V_2}{\partial\xi\partial\eta}=Nl_1(W_1), \tag{62a}$$

$$\frac{1+\mu}{2}\frac{\partial^2U_2}{\partial\xi\partial\eta}+\frac{1-\mu}{2}\frac{\partial^2V_2}{\partial\xi^2}+\frac{\partial^2V_2}{\partial\eta^2}=Nl_2(W_1). \tag{62b}$$

It is possible to reduce Eq. (62) with any of the boundary conditions (15)–(19) to a variational problem considering the minimum of energy integral [39] and developing U_2 and V_2 in a series of functions that satisfy the geometrical boundary conditions; this gives

$$I = \int_\Omega \left\{ \left(\frac{\partial U_2}{\partial \xi}\right)^2 + \left(\frac{\partial V_2}{\partial \eta}\right)^2 + 2\mu \frac{\partial U_2}{\partial \xi}\frac{\partial V_2}{\partial \eta} + \frac{1-\mu}{2}\left(\frac{\partial U_2}{\partial \eta} + \frac{\partial V_2}{\partial \xi}\right)^2 - 2\left[\frac{\partial W_1}{\partial \xi}\frac{\partial^2 W_1}{\partial \xi^2} + \frac{1+\mu}{2}\frac{\partial W_1}{\partial \eta}\frac{\partial^2 W_1}{\partial \xi \partial \eta} + \frac{1-\mu}{2}\frac{\partial W_1}{\partial \xi}\frac{\partial^2 W_1}{\partial \eta^2}\right] U_2 - 2\left[\frac{\partial W_1}{\partial \eta}\frac{\partial^2 W_1}{\partial \eta^2} + \frac{1+\mu}{2}\frac{\partial W_1}{\partial \xi}\frac{\partial^2 W_1}{\partial \xi \partial \eta} + \frac{1-\mu}{2}\frac{\partial W_1}{\partial \eta}\frac{\partial^2 W_1}{\partial \xi^2}\right] V_2 \right\} d\Omega - \int_{\partial\Omega} \left(U_{2n}\left(\left(\frac{\partial W}{\partial n}\right)^2 + \mu\left(\frac{\partial W}{\partial \tau}\right)^2\right) + (1-\mu) V_{2n}\frac{\partial W}{\partial n}\frac{\partial W}{\partial \tau}\right) dS, \quad (63)$$

where $U_{2n} = U_2 l + V_2 m$, $V_{2n} = -U_2 m + V_2 l$, l and m being the directional cosines that can be obtained by using the R-function ω [29]: $l = -(\partial\omega/\partial\xi)$, $\quad m = -(\partial\omega/\partial\eta)$.

In particular, Eq. (63) takes a simplified expression for clamped edges, as a consequence that the last integral in Eq. (63) (extended to the boundary $\partial\Omega$) vanishes. The Ritz method is used to discrete Eq. (63). In particular, $U_2(\xi, \eta)$ and $V_2(\xi, \eta)$, defined in a domain of arbitrary shape, are expanded by using the R-functions theory. Eqs. (49–53), constructed for $U_1(\xi, \eta)$ and $V_1(\xi, \eta)$, can now be used to obtain $U_2(\xi, \eta)$ and $V_2(\xi, \eta)$.

7. Numerical results

Eigenvalues and eigenvectors of linear vibrations of shallow shells, as well as the functions $U_2(\xi, \eta)$, $V_2(\xi, \eta)$ and the coefficients α and β in Eq. (23), have been calculated by using the computer program POLYE–RL [40]. The resulting second-order nonlinear differential Eq. (23) is integrated by using the 5th order Runge–Kutta method in the commercial computer program MAPLE. All the nonlinear results are obtained for the vibration mode with one longitudinal half-wave in both x and y directions, briefly indicated as mode (1,1). In the presentation of numerical results, the sign of the flexural displacement W has been changed in order to have positive displacements outward the shell and negative displacements inwards, in order to be consistent with the results in Ref. [34].

7.1. Numerical results for circular cylindrical panels with rectangular base

Numerical results have been obtained for free vibrations of circular cylindrical panels by using the RFM. Curved panels with rectangular base are initially considered. Numerical results present the backbone curves, indicating the change in the resonance frequency versus the vibration amplitude; the backbone curves (amplitude–frequency curves) shown are relative to the maximum vibration amplitude outwards (i.e. on the side of the panel opposite to the center of curvature; this amplitude is different with respect to vibration amplitude inwards in negative direction of the z-axis, which is larger in amplitude), measured in radial direction at the center of the panel. Several types of boundary conditions are considered. The ten dots Gauss quadrature formula has been used to perform numerical double integrals.

Example 1. A circular cylindrical panel with rectangular base, having the dimension ratios $a/b = 1$, $h/R_x = 0.001$, $a/R_x = 0.4$ and Poisson ratio $\mu = 0.3$ is investigated. Calculations have been performed for classical simply supported edges. The same panel was previously studied by Leissa and Kadi [12], and Chia [17].

Fig. 3 shows the comparison of the backbone curve obtained in the present study with those given in Refs. [12,17], also obtained by using a single dof and the same shell theory neglecting in-plane inertia. The present results are in reasonable agreement with those in Refs. [12,17] for vibration amplitudes up to three times the panel thickness, being closer to those in Ref. [12].

In order to verify the accuracy of the method, the natural frequency of the mode (1,1) is given in Table 1. The convergence of the natural frequency with the number N_3 of terms in Eq. (59c) is shown and results are

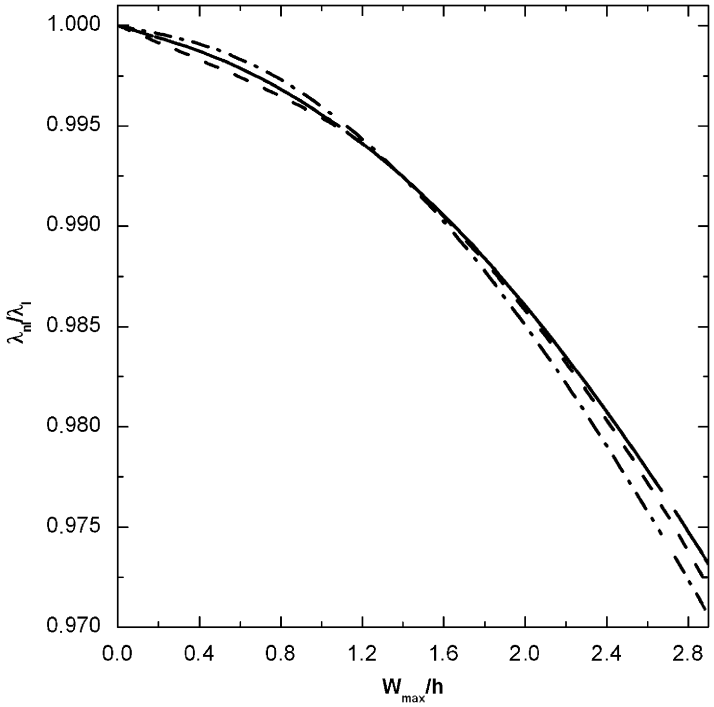

Fig. 3. Amplitude–frequency curves for the fundamental mode of panels with square base ($b/a = 1$, $R_x/a = 2.5$, $h/R_x = 0.001$, $\mu = 0.3$); —, RFM; ----, backbone curve from Chia [17]; – · – ·, backbone curve from Leissa and Kadi [12].

Table 1

Non-dimensional frequency parameter $\omega_0\sqrt{\rho(1-\mu^2)R_x^2/E}$ of free vibrations of the panel ($a/b = 1$, $h/R_x = 0.001$, $a/R_x = 0.4$, $\mu = 0.3$); convergence of the present solution (RFM) with the total number of terms in the expansions and reference solution [12]

Ref. [12]	RFM: number of terms in the expansions				
	18	30	45	63	84
0.47555	0.47556	0.47556	0.47555	0.47555	0.47555

compared to the frequency obtained by Leissa and Kadi [12]. It can be observed in Table 1 that the non-dimensional frequency parameter computed with 45 terms converges to the value obtained by Leissa and Kadi [12]. Increasing the number of terms up to 84 does not make any significant change in the results.

A good agreement of the present results, both linear in Table 1 and nonlinear in Fig. 3, with those in Ref. [12] shows the accuracy of the present approach.

Example 2. A shallow circular cylindrical panel with boundary conditions given by Eqs. (15)–(18), having dimension ratios $b/a = 1$, $R_x/a = 10$, $h/a = 0.01$, $\mu = 0.3$, is considered. Free nonlinear vibrations of the panel, classical simply supported at four edges, were previously investigated by Kobayashi and Leissa [11]. A very good agreement of the backbone curves obtained in the present study with the one obtained in Ref. [11] is shown in Fig. 4 for classical simply supported edges.

Fig. 5 shows the backbones curves of the panel for four different types of boundary conditions; both the maximum, Fig. 5(a), and the minimum, Fig. 5(b), of the panel response are shown. It is interesting to note that the backbone curve obtained for in-plane free simply supported panel, Eq. (18), shows always hardening type nonlinearity; this is similar to the case of clamped panel, Eq. (15). For other types of boundary conditions, Eqs. (16) and (17), softening type nonlinearity is initially obtained, quickly turning to hardening type. It can be

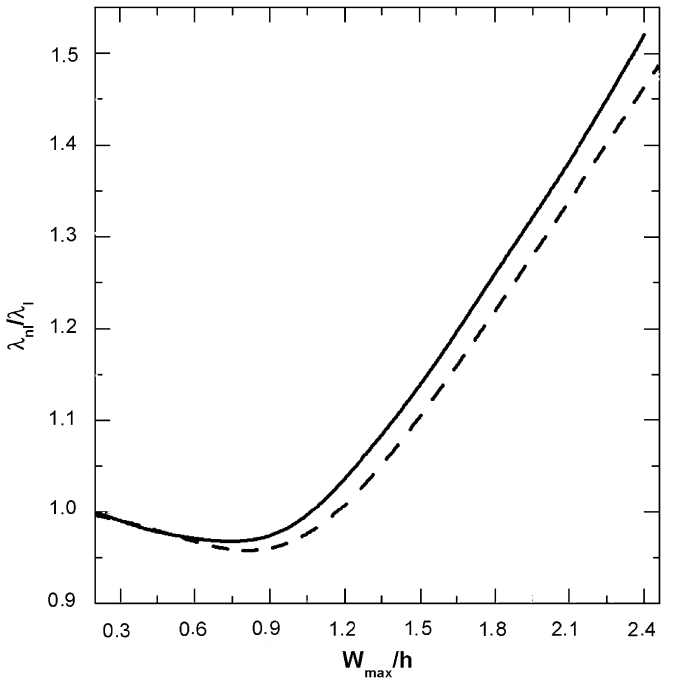

Fig. 4. Amplitude–frequency curves for panels of rectangular base ($b/a = 1$, $R_x/a = 10$, $h/R_x = 0.01$, $\mu = 0.3$); —, RFM; ----, backbone curve from Kobayashi and Leissa [11].

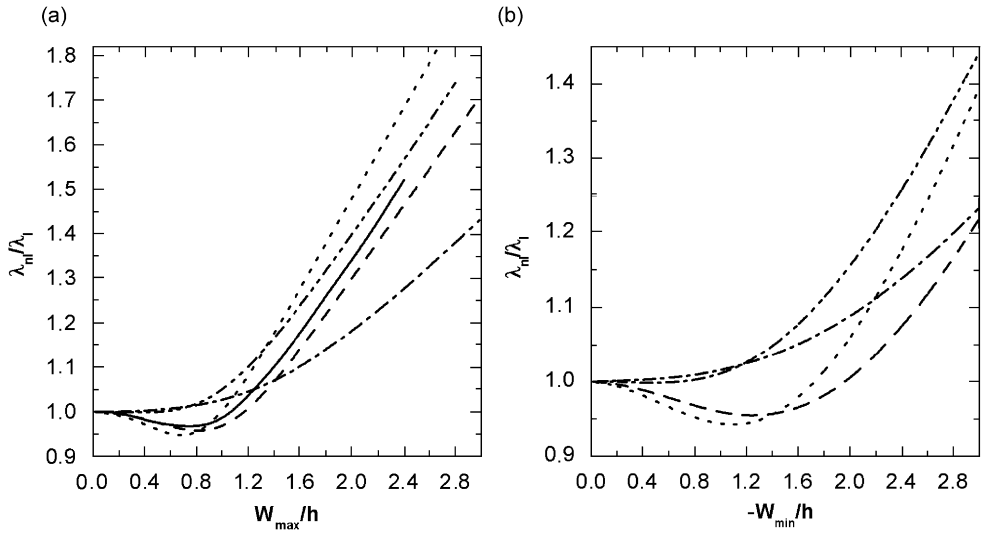

Fig. 5. Effect of boundary conditions on amplitude–frequency curves for panels of rectangular base ($b/a = 1$, $R_x/a = 10$, $h/R_x = 0.01$, $\mu = 0.3$); —, classical simply supported panel, [11]; - - -, classical simply supported edges, RFM; · · · · · ·, in-plane immovable simply supported edges, RFM; – · – · –, in-plane free simply supported edges, RFM; – · · · – · · –, clamped edges, RFM. (a) Maximum of the coordinate w in a vibration period; (b) minus minimum of coordinate w.

observed that, excluding the clamped case where the rotational constraints play a fundamental role deforming the fundamental mode shape and largely increasing its natural frequency, in-plane constraints change the nonlinearity from hardening (in-plane free edges) to softening (simply supported and in-plane immovable) due to the increased importance of in-plane stretching with respect to bending.

Table 2
Natural frequency ω_0 (Hz) of the panel with rectangular base for different boundary conditions ($a = b = 0.1\,\text{m}$, $R_x = 1\,\text{m}$, $h = 0.001\,\text{m}$, $E = 206 \times 10^9\,\text{Pa}$, $\rho = 7800\,\text{kg/m}^3$, $\mu = 0.3$)

Boundary conditions	RFM (Hz)	Ref. [34] (Hz)
In-plane free simply supported	535.0	539.4
Classical simply supported	637.0	636.9
In-plane immovable simply supported	911.9	912.0
Clamped	1145.5	1168.3

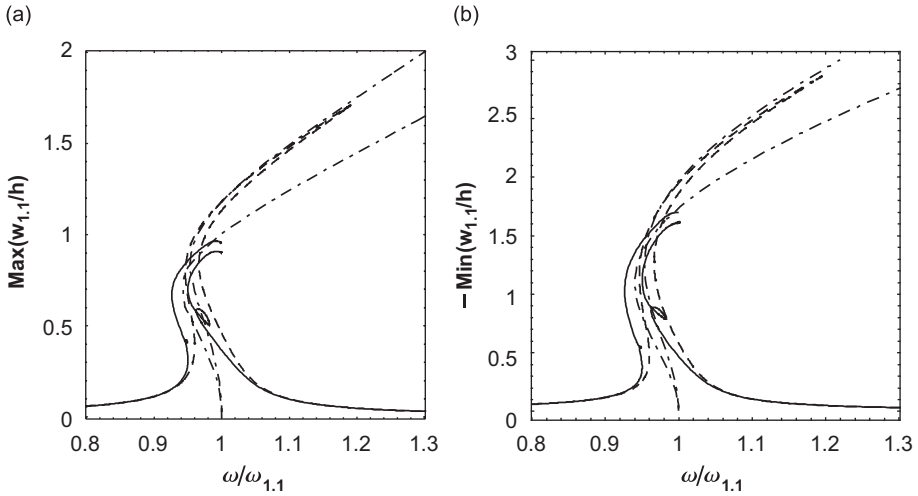

Fig. 6. Amplitude of the response of the panel with rectangular base vs. the excitation frequency; —, classical simply supported edges [34]; ----, in-plane immovable simply supported edges [34]; – · – ·, backbone curves (RFM). (a) Maximum of the coordinate w in a vibration period; (b) minus minimum of coordinate w.

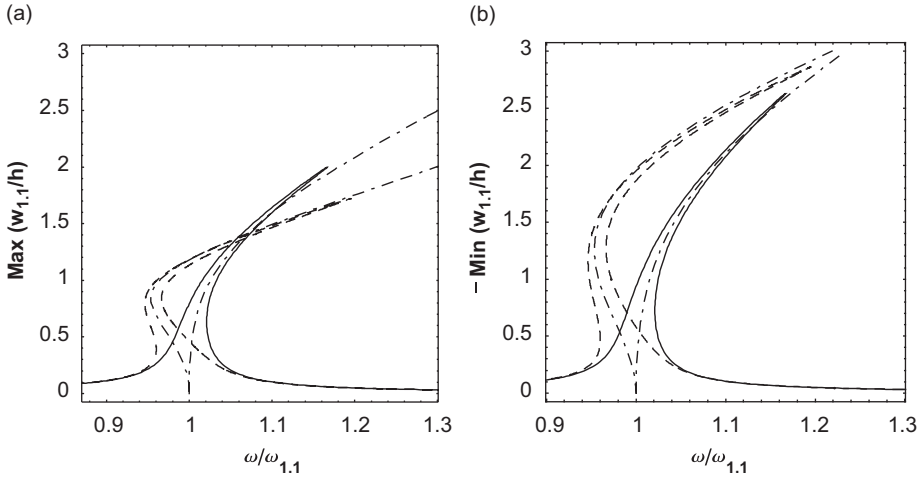

Fig. 7. Amplitude of the response of the panel with rectangular base vs. the excitation frequency; —, in-plane free simply supported edges [34]; ---, classical simply supported edges [34]; – · – ·, backbone curves (RFM). (a) Maximum of the coordinate w in a vibration period; (b) minus minimum of coordinate w.

Example 3. Free vibrations of a shallow circular cylindrical panel with different boundary conditions are considered. The panel has the following dimension and material properties: length between supports $b = 0.1\,\text{m}$, curvilinear dimension $a = 0.1\,\text{m}$, radius of curvature $R_x = 1\,\text{m}$, thickness $h = 0.001\,\text{m}$, Young's

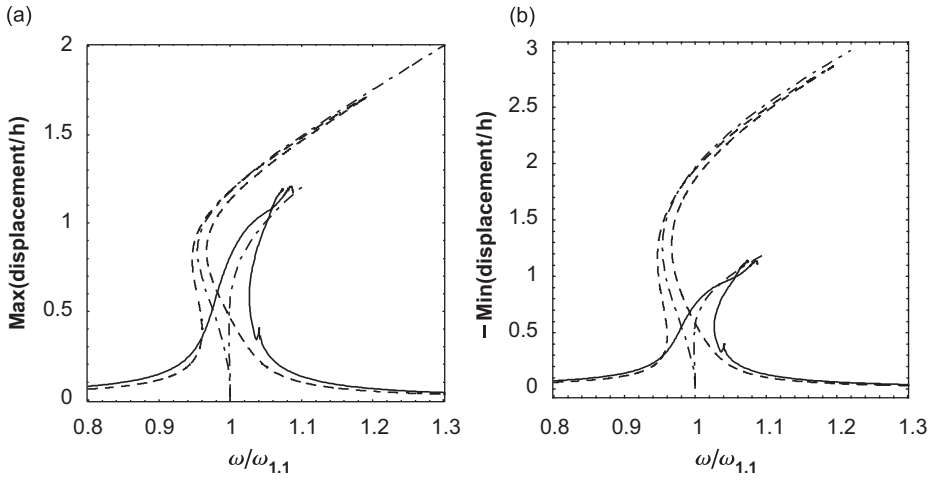

Fig. 8. Amplitude of the response of the panel with rectangular base vs. the excitation frequency; - - -, classical simply supported edges [34]; —, clamped edges [34]; – · – ·, backbone curves (RFM). (a) Maximum of the displacement w at the center of the panel in a vibration period; (b) minus minimum of displacement w at the center of the panel.

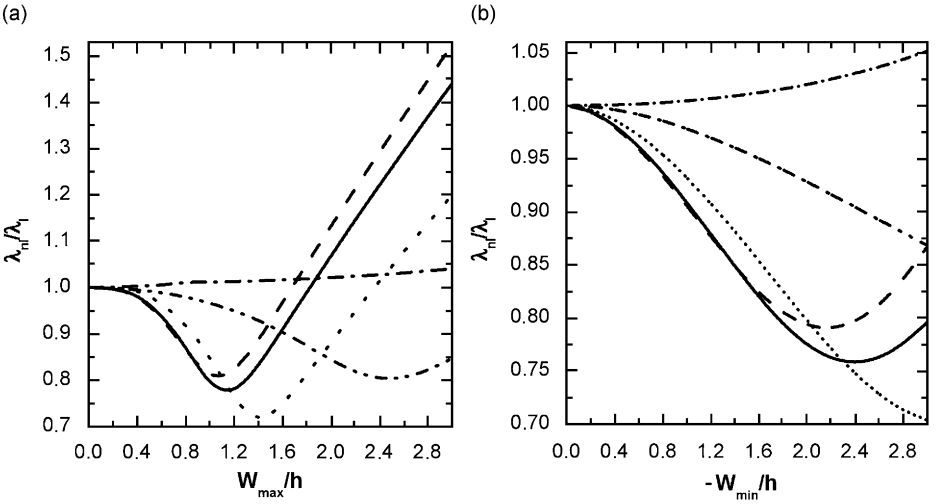

Fig. 9. Effect of boundary conditions on amplitude–frequency curves for the panel with complex base in Fig. 2; RFM solution; —, clamped edges; - - -, in-plane immovable simply supported edges; · · · ·, classical simply supported panel; – · – ·, in-plane free simply supported edges; – · · – · ·, in-plane free simply supported edges with additional distributed elastic tangential spring of stiffness per unit length $k_{spr} = 75*10^{11}\,\mathrm{N/m^2}$. (a) Maximum of the coordinate w in a vibration period; (b) minus minimum of coordinate w.

modulus $E = 206\,\mathrm{GPa}$, mass density $\rho = 7800\,\mathrm{kg/m^3}$ and Poisson ratio $\mu = 0.3$. The panel with the same dimension ratios ($b/a = 1$, $R_x/a = 10$, $h/R_x = 0.01$, $\mu = 0.3$) was previously studied in Ref. [11] with classical simply supported edges, and in the present study, Example 2, for four types of boundary conditions (see Fig. 5). The same panel subjected to forced vibration with non-dimensional harmonic force excitation $f = 0.021$ (defined in Ref. [34] and corresponding to 6.6 N for simply supported panel) applied at the center of the panel and damping ratio $\zeta = 0.004$ has been recently studied by Amabili [34], by using also a model previously developed in Ref. [21], for different boundary conditions with a different approach and by using up to 39 dof in the nonlinear models, which are based on Donnell's nonlinear shell theory retaining in-plane inertia.

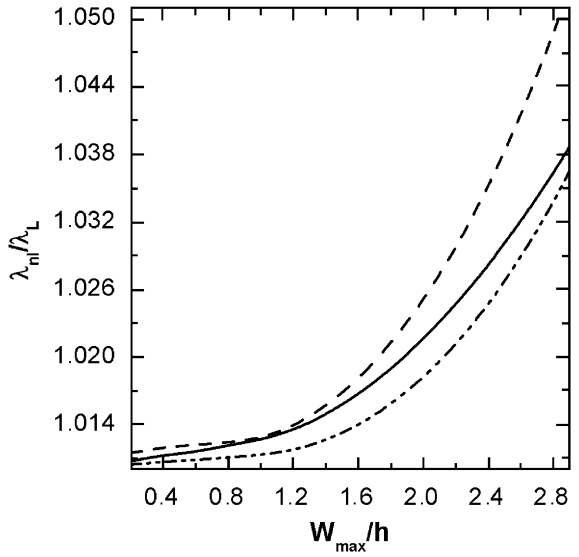

Fig. 10. Amplitude–frequency curves of the panel with complex shape for various cut depths ratios a_1/a, RFM; —, $a_1/a = 0.7$; ---, $a_1/a = 0.8$; – · · –, $a_1/a = 0.9$.

The natural frequency ω_0 of the fundamental mode of the panel for four different boundary conditions has been computed by the RFM and compared in Table 2 to results presented by Amabili [34]; a very good agreement of the results confirms the accuracy of the present approach.

Figs. 6–8 show the maximum (part (a) of the figures) and minimum (part (b) of the figures) of the panel radial response of the fundamental mode versus the excitation frequency computed by Amabili [34] for each of the four types of boundary conditions given in Eqs. (15)–(18); results are compared to those obtained by using the RFM, where only backbone curves have been computed. The present results for free vibration are extremely close to those of Amabili [34], as shown in Figs. 6–8, for all the considered boundary conditions; this gives an excellent agreement. In order to perform the comparison, it is necessary to consider that the backbone curve approximately goes through the middle of the forced response curves for different force levels.

7.2. Numerical results for circular cylindrical panels with complex base

A circular cylindrical panel with complex base, shown in Fig. 2, is investigated. The dimension and material properties of the panel are assumed to be (see Fig. 2): overall length $b = 0.199\,\text{m}$, curvilinear width $a = 0.132\,\text{m}$, length of the cut $b_1 = 0.041\,\text{m}$, curvilinear width at the cut $a_1 = 0.092\,\text{m}$, radius of curvature $R_x = 2\,\text{m}$, thickness $h = 0.00028\,\text{m}$, Young's modulus $E = 195\,\text{GPa}$, mass density $\rho = 7800\,\text{kg/m}^3$, Poisson ratio $\mu = 0.3$.

Fig. 9 shows the backbone curve of the panel calculated in the present study by using the RFM for each of the five types of boundary conditions given in Eqs. (15)–(19); the maximum, Fig. 9(a), and the minimum, Fig. 9(b), of the response at the center of the panel, in radial direction, are shown. It is interesting to note that, in the case of in-plane free simply supported edges of the panel, results indicate very weak hardening type nonlinearity. The backbone curves for the other types of boundary conditions indicate softening type nonlinearity.

Numerical calculations have been performed for the same panel as the cut depth approaches $a_1/a \to 1$, i.e. approaches the limit case of a panel with rectangular base; boundary conditions are in-plane free simply supported at all the edges. The influence of the cut depth on the nonlinear amplitude–frequency curve of the panel is shown in Fig. 10. Globally 63 terms have been used in the expansions in order to get the results presented. This number of terms corresponds to the eleventh power in the polynomials approximating U and V, and to the tenth power in the polynomial approximating W in Eqs. (59a–c); this number of terms has been found to give convergence of the linear eigenfunctions and eigenvectors.

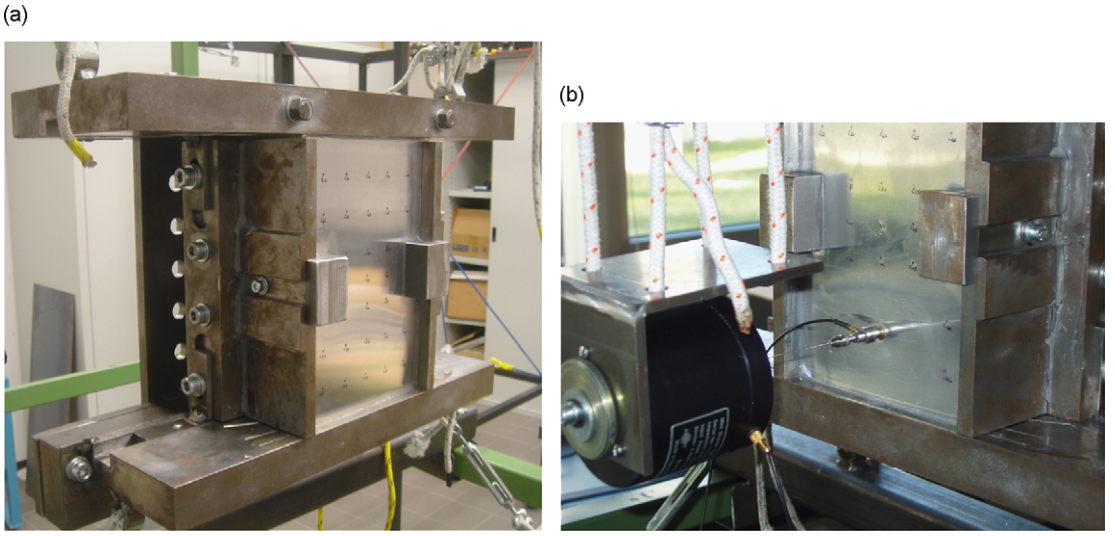

Fig. 11. Experimental set-up. (a) Curved panel with complex base; (b) panel excited by the shaker at $\tilde{x} = 40\,\text{mm}$ and $\tilde{y} = a/2$.

8. Experimental results and comparison

Tests have been conducted on an aluminum circular cylindrical panel with the same geometry (but different material) used for calculation in Section 7.2: $b = 0.199\,\text{m}$, $a = 0.132\,\text{m}$, $b_1 = 0.041\,\text{m}$, $a_1 = 0.092\,\text{m}$, $R_x = 2\,\text{m}$, $h = 0.00028\,\text{m}$, $E = 70\,\text{GPa}$, $\rho = 2700\,\text{kg/m}^3$, $\mu = 0.33$. The panel was inserted into a heavy rectangular steel frame, see Fig. 11, having V-grooves designed to hold the panel and to avoid transverse (radial) displacements at the edges; silicon was placed into the grooves to fill any gap between the panel and the grooves. In-plane displacements normal to the edges were allowed on the convex part of the domain because the constraint given by silicon on these displacements was very small; this may be not true for the concave part of the domain; in-plane displacements parallel to the edges were elastically constrained by the silicon. Therefore, the experimental boundary conditions are close to those given for in-plane free, simply supported boundary conditions with distributed springs parallel to the edges, as expressed by Eq. (19), at least for the convex part of the panel; for the two concave parts the same boundary conditions are imposed to the model, but the actual constraints in the tested plate are probably more complex.

The panel has been subjected to: (i) burst-random excitation to identify the natural frequencies and perform a modal analysis by measuring the panel response on a grid of points, (ii) harmonic excitation, increasing or decreasing by very small steps the excitation frequency in the spectral neighborhood of the fundamental natural frequency, to characterize nonlinear responses in presence of large-amplitude vibrations (step-sine excitation). The excitation has been provided by an electrodynamical exciter (shaker), model *B&K* 4810. A piezoelectric miniature force transducer *B&K* 8203 of the weight of 3.2 g, glued to the panel and connected to the shaker with a stinger, measured the force transmitted. The panel response has been measured by using a very accurate laser Doppler vibrometer Polytec (sensor head OFV-505 and controller OFV-5000) in order to have non-contact measurement without introduction of inertia. The time responses have been measured by using the Difa Scadas II front-end, connected to a HP c3000 workstation, and the software CADA-X 3.5b of LMS for signal processing, data analysis, experimental modal analysis and excitation control. The same front-end has been used to generate the excitation signal. The CADA-X closed-loop control has been used to keep constant the value of the excitation force for any excitation frequency, during the measurement of the nonlinear response.

The measured natural frequency of the fundamental mode (1,1), which is the only one investigated in the present study, is 156 Hz. The measured excitation was far from being sinusoidal; as usual, higher harmonics are introduced by the shaker around resonance for higher excitation levels [41].

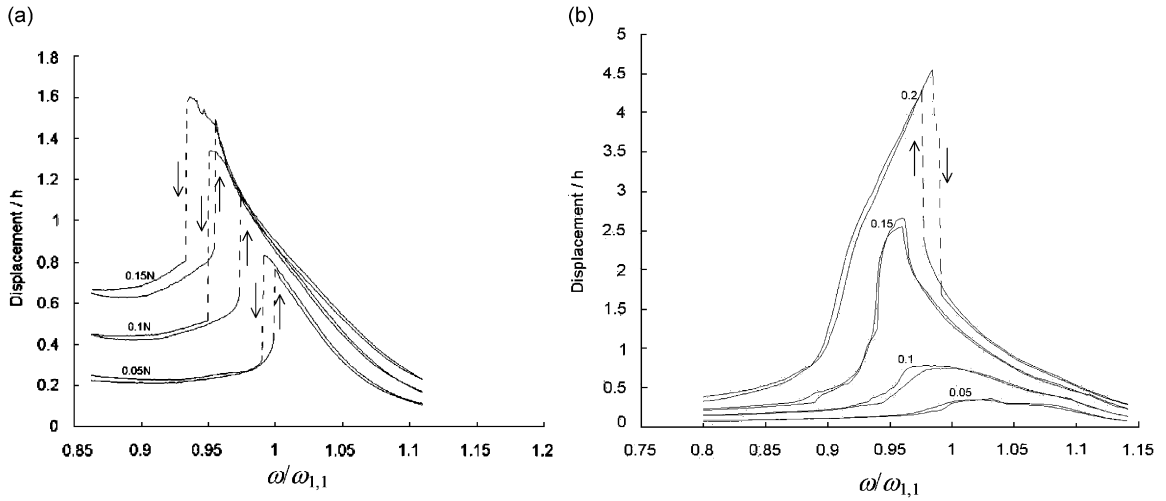

Fig. 12. Experimental oscillatory displacement (1st harmonic) vs. excitation frequency for different excitation levels measured at the center of the panel; fundamental mode (1,1). —— experimental points;- -, connecting line; →, direction of movement along the line. (a) Excitation at $\tilde{x} = 40\,\text{mm}$ and $\tilde{y} = a/2$; (b) excitation at a different position.

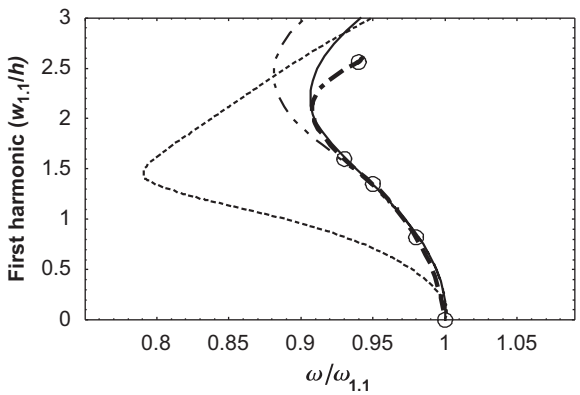

Fig. 13. Comparison of numerical (for different stiffness values k_{spr}) and experimental amplitude–frequency curves (1st harmonic) of the panel with complex shape; fundamental mode (1,1). ○, Experimental value; – · –, line interpolating the experimental data; - -, simply supported panel ($k_{\text{spr}} \to \infty$); – · –, $k_{\text{spr}} = 197 \times 10^{11}\,\text{N/m}^2$; ——, $k_{\text{spr}} = 52.6 \times 10^{11}\,\text{N/m}^2$.

Fig. 12(a) shows the measured forced oscillation (displacement, directly measured by using the Polytec laser Doppler vibrometer with displacement decoder DD-200 in the OFV-5000 controller; measurement position at the center of the panel) around the fundamental frequency, i.e. mode (1, 1), vs. the excitation frequency for three different force levels: 0.05, 0.1, and 0.15 N. The excitation point was at $\tilde{x} = 40\,\text{mm}$ and $\tilde{y} = a/2$. Fig. 12(b) shows the measured forced oscillation around the fundamental frequency vs. the excitation frequency for four different force levels: 0.05, 0.1, 0.15 and 0.2 N for a different position of the excitation point. The closed-loop control used in the experiments keeps constant the amplitude of the harmonic excitation force, after filtering the signal from the load cell in order to use only the harmonic component with the given excitation frequency. The measured oscillation reported in Fig. 12 has been filtered in order to eliminate any frequency except the excitation frequency (1st harmonic of the response). Experiments have been performed increasing and decreasing the excitation frequency (up and down); the frequency step used in this case is 0.02 Hz, 16 periods have been measured with 128 points per period and 200 periods have been skipped before data acquisition every time that the frequency is changed. In Fig. 12(a) the hysteresis between

the two curves (up = increasing frequency; down = decreasing frequency) is clearly visible. Sudden increments (jumps) of the vibration amplitude are observed when increasing and decreasing the excitation frequency; these indicate softening-type nonlinearity. However, in Fig. 12(b), it is shown that for larger vibration amplitude there is a folding, and the nonlinear behavior turns to hardening-type.

By using the forced responses in Figs. 12(a, b), the experimental backbone curve, indicating the frequency–amplitude relationship in case of free vibrations, is obtained. This curve is plotted in Fig. 13 vs. the theoretical calculations for aluminum panels with simply supported edges and in-plane free simply supported edges with additional elastic tangential spring of stiffness k_{spr}. The theoretical first-harmonic component is plotted, which is approximately the average value between the oscillation amplitude outside and inside the shell. In particular, the theoretical curve for $k_{spr} = 52.6 \times 10^{11}\,\mathrm{N/m^2}$ is extremely close to the experimental results, giving both a qualitative and quantitative validation of the theoretical approach. However, the natural frequency computed for $k_{spr} = 52.6 \times 10^{11}\,\mathrm{N/m^2}$ is significantly larger than the measured one (156 Hz). However, for $k_{spr} = 0.63 \times 10^{11}\,\mathrm{N/m^2}$ a computed natural frequency of 160 Hz is obtained, which is extremely close to the experimental value. The indetermination of the experimental boundary conditions as well as a significant effect of geometric imperfections on both natural frequency and trend of nonlinearity are the probable reason for differences between numerical and experimental results; geometric imperfections are not taken into account in the present study.

9. Conclusions

In the present study, geometrically nonlinear vibrations of circular cylindrical panels with different shape of the boundary are considered for several boundary conditions. The study of the nonlinear vibrations is based on the R-functions theory and variational methods, which allow considering complex shape of the panels.

Numerical calculations of nonlinear free vibrations of circular cylindrical shells with rectangular base have been performed for several sets of boundary conditions. In order to check the accuracy of the present approach, a comparison with the natural frequencies, backbone curves and forced responses previously obtained by Amabili [34], Kobayashi and Leissa [11] and Leissa and Kadi [12] has been carried out. Free vibrations of circular cylindrical panels with complex geometry have been investigated by using the RFM. Specific laboratory experiments have been conducted on a panel having the same geometry in order to give a further validation of the numerical results.

References

[1] Ya.M. Grigorenko, V.I. Guljaev, Nonlinear problems of the shells theory and methods of their solution (review), *Prikladnaya Mekhanika* 27 (1991) 3–23 (in Russian).
[2] V.D. Kubenko, P.S. Koval'chuk, Nonlinear problems of the vibration of thin shells (review), *International Applied Mechanics* 34 (1998) 703–728.
[3] M. Amabili, M.P. Païdoussis, Review of studies on geometrically nonlinear vibrations and dynamics of circular cylindrical shells and panels, with and without fluid–structure interaction, *Applied Mechanics Reviews* 56 (2003) 349–381.
[4] A.S. Volmir, *Nonlinear Dynamics of Plates and Shells*, Nauka, Moscow, Russia, 1972 (in Russian).
[5] A.S. Volmir, A.A. Logvinskaya, V.V. Rogalevich, Nonlinear natural vibrations of rectangular plates and cylindrical panels, *Soviet Physics– Doklady* 17 (1973) 720–721.
[6] E.I. Grigolyuk, Nonlinear vibrations and stability of shallow shells and beams, *Izvestiya of Academy of Science of the USSR, Mekhanika and Mechanical Engineering* 3 (1955) 33–68 (in Russian).
[7] E.I. Grigolyuk, Vibrations of circular cylindrical panels subjected to finite deflections, *Prikladnaya Matematika i Mekhanika* 19 (1955) 376–382 (in Russian).
[8] E. Reissner, Nonlinear effects in vibrations of cylindrical shells, Ramo–Wooldrige Corporation Report AM5-6, 1955.
[9] B.E. Cummings, Large-amplitude vibration and response of curved panels, *AIAA Journal* 2 (1964) 709–716.
[10] N.N. Bogolyubov, Yu.A. Mitropolski, *The Asymptotic Methods in the Theory of Nonlinear Vibrations*, Nauka, Moscow, Russia, 1974 (in Russian).
[11] Y. Kobayashi, A.W. Leissa, Large amplitude free vibration of thick shallow shells supported by shear diaphragms, *International Journal of Non-Linear Mechanics* 30 (1995) 57–66.
[12] A.W. Leissa, A.S. Kadi, Curvature effects on shallow shell vibrations, *Journal of Sound and Vibration* 16 (1971) 173–187.
[13] Yu.V. Samoylov, About the accuracy ranking of approximate solutions in problems of nonlinear vibrations of shells, *Stroitelnaya Mekhanika i Raschet Sooruzheniy* 6 (1971) 37–41 (in Russian).

[14] R.A. Raouf, A qualitative analysis of the nonlinear dynamic characteristics of curved orthotropic panels, *Composites Engineering* 3 (1993) 1101–1110.
[15] A.A. Popov, J.M.T. Thompson, J.G.A. Croll, Bifurcation analyses in the parametrically excited vibrations of cylindrical panels, *Nonlinear Dynamics* 17 (1998) 205–225.
[16] E.H. Dowell, C.S. Ventres, Modal equations for the nonlinear flexural vibrations of a cylindrical shell, *International Journal of Solids and Structures* 4 (1968) 975–991.
[17] C.Y. Chia, Nonlinear analysis of doubly curved symmetrically laminated shallow shells with rectangular platform, *Ingenieur-Archiv* 58 (1988) 252–264.
[18] Y.M. Fu, C.Y. Chia, Multi-mode nonlinear vibration and postbuckling of anti-symmetric imperfect angle-ply cylindrical thick panels, *International Journal of Non-Linear Mechanics* 24 (1989) 365–381.
[19] C.Y. Chia, Nonlinear free vibrations and postbuckling of symmetrically laminated orthotropic imperfect shallow cylindrical panels with two adjacent edges simply supported and the other edges clamped, *International Journal of Solids and Structures* 23 (1987) 1123–1132.
[20] A. Abe, Y. Kobayashi, G. Yamada, Non-linear vibration characteristics of clamped laminated shallow shells, *Journal of Sound and Vibration* 234 (2000) 405–426.
[21] M. Amabili, Nonlinear vibrations of circular cylindrical panels, *Journal of Sound and Vibration* 281 (2005) 509–535.
[22] M. Amabili, Nonlinear vibrations of doubly curved shallow shells, *International Journal of Non-Linear Mechanics* 40 (2005) 683–710.
[23] N.A. Alumjae, The transforming processes of deformation of flexible shells and plates, *Proceedings of the Sixth Union Conference on The Shells and Plates Theory*, Nauka, 1966, pp. 833–889 (in Russian).
[24] M. Amabili, Comparison of shell theories for large amplitude vibrations of circular cylindrical shells: Lagrangian approach, *Journal of Sound and Vibration* 264 (2003) 1091–1125.
[25] F.B. Badalov, G.S. Shadmanov, N.J. Huzhajarov, Vibrations of viscoelastic plates and shallow shells with physically and geometrically nonlinear characteristics, *Mekhanika Deformiruemogo tverdogo tela* (1981) 35–42 (in Russian).
[26] F.B. Badalov, H. Eshmatov, B. Anzhiev, Research of physically and geometrically nonlinear vibrations of viscoelastic plates and shells by the method of averaging, *Prikladnaya Mekhanika* 21 (1985) 61–68 (in Russian).
[27] V.N. Pastushihin, Free vibrations of nonlinear viscoelastic shells, *Prikladnaya Mekhanika* 7 (1971) 16–20 (in Russian).
[28] V.L. Rvachev, *Theory of* R-fun*ctions and Some of its Applications*, Nauka Dumka, Kiev, Ukraine, 1982 (in Russian).
[29] V.L. Rvachev, L.V. Kurpa, *The* R-fun*ctions in Problems of Plate Theory*, Nauka Dumka, Kiev, Ukraine, 1987 (in Russian).
[30] V.L. Rvachev, L.V. Kurpa, The application of the R-functions theory for the investigation of plates and shells of arbitrary shape, *Problems of Machine– Building* 1 (1998) 33–53 (in Russian).
[31] L.V. Kurpa, V.L. Rvachev, E. Ventsel, The R-function method for the free vibration analysis of thin orthotropic plates of arbitrary shape, *Journal of Sound and Vibration* 261 (2003) 109–122.
[32] L.V. Kurpa, G. Pilgun, E. Ventsel, Application of the R-function method to nonlinear vibrations of thin plates of arbitrary shape, *Journal of Sound and Vibration* 284 (2005) 379–392.
[33] L.V. Kurpa, K.I. Lyubitska, A.V. Shmatko, Solution of vibration problems for shallow shells of arbitrary form by the R-function method, *Journal of Sound and Vibration* 279 (2005) 1071–1084.
[34] M. Amabili, Effect of boundary conditions on nonlinear vibrations of circular cylindrical panels, *Transactions of the ASME, Journal of Applied Mechanics*, 74 (2007) 645–657.
[35] V.L. Rvachev, T.I. Sheiko, V. Shapiro, I. Tsukanov, On completeness of RFM solution structures, *Computational Mechanics* 25 (2000) 305–316.
[36] V.L. Rvachev, T.I. Sheiko, R-functions in boundary value problems in mechanics, *Applied Mechanics Review* 48 (1995) 151–188.
[37] L.V. Kantorovich, V.I. Krylov, *Approximate Methods of Higher Analysis*, Interscience Publisher, New York, 1958.
[38] V.L. Rvachev, Analytical description of some geometric objects, *Doklady AS USSR* 153 (1963) 765–768 (in Russian).
[39] S.G. Mikhlin, *Variational Methods in Mathematical Physics*, Pergamon Press, Oxford, UK, 1964.
[40] V.L. Rvachev, A.N. Shevchenko, *Problem-oriented Languages and Systems for Engineering Approaches*, Tekhnika, Kiev, Ukraine, 1988 (in Russian).
[41] M. Amabili, Theory and experiments for large-amplitude vibrations of circular cylindrical panels with geometric imperfections, *Journal of Sound and Vibration* 298 (2006) 43–72.